International Journal of Mechanical Sciences 304 (2025) 110683



Contents lists available at ScienceDirect

International Journal of Mechanical Sciences

journal homepage: www.elsevier.com/locate/ijmecsci





Temperature effect on dynamic translaminar fracture of thermoplastic composites

Gustavo Quino [a,b,*], Karthik Ram Ramakrishnan [b]

[a] Department of Aeronautics, Imperial College London, SW7 2AZ, UK
[b] Bristol Composites Institute, University of Bristol, BS8 1TR, UK

ARTICLE INFO

Keywords:
Composites
Fracture
Thermoplastic
Translaminar fracture toughness
High strain rate
CF/PEEK

ABSTRACT

Carbon fibre thermoplastic composites are emerging as an attractive alternative to thermoset composites for next-generation aerospace applications due to combination of manufacturing efficiency, mechanical performance, weight reduction, and sustainability benefits. The damage-tolerance of thermoplastic composite structures is influenced by their translaminar fracture toughness. Although temperature is known to influence the properties of these composites, its impact in the dynamic regime—particularly on the translaminar energy release rate related to fibre fracture—has not been extensively studied. This study shows, for the first time, the experimental characterisation of the dynamic mode-I translaminar critical energy release rate at various temperatures for a carbon fibre PEEK composite. An adaptation of the split Hopkinson pressure bar system was used to conduct compact tension experiments at high loading rates. Digital image correlation (DIC) analysis on ultra high-speed images was employed to extract the strain fields, crack tip location and the opening displacements in the different cases. By using the area method to evaluate the fracture energies, we found that the worst case for dynamic fracture, where the critical energy release rate was found to be minimum, was at 90 °C, showing 27 % lower energy than at room temperature. Specimens tested at -55 °C showed no significant difference to the room temperature high-rate experiments. DIC, micro-CT and SEM imaging offered insights on the underlying mechanisms behind these experimental observations.

1. Introduction

The demand for high performance composite structures in aerospace and automotive industries is continuously growing. This is primarily driven by their high specific strength and the potential for lifetime greenhouse gas emissions reduction due to lightweighting. However, most of the composites in service are made with thermoset matrix systems such as epoxy and are hard to recycle at their end of life because of their high crosslinking. In recent years, the interest in repairability and recyclability of composites have motivated the exploration of thermoplastic matrix composites [1–4]. The ability to remelt and reshape thermoplastics allows for easier repairs and recycling. Parts can also be manufactured in minutes rather than hours, with up to 80 % reduction in manufacturing cycle times. The ductility of the thermoplastic matrix has been shown to improve toughness and damage tolerance of composites [5]. Carbon fibre reinforced thermoplastic composites (CFRTP) with a wide range of engineering thermoplastics such as polyamide (PA), polycarbonate (PC), polyetheretherketone (PEEK), polyetherimide (PEI), and polyethersulfone (PES) have been studied [6–8]. The combination of high strength, stiffness, and resistance to wear and fatigue make carbon fibre PEEK composites (CF/PEEK) an attractive material for a wide range of applications where high-performance and durability are required [2,3,9].

There are some papers that have studied the strain rate effects on the stiffness and strength properties of CFRTPs [10–12]. It is well reported that the mechanical behaviour of CF/PEEK composites is influenced by loading rate and temperature due to the existence of thermal transitions in polymer behaviour [13]. PEEK typically exhibits a decrease in stiffness and an increase in ductility with increasing temperature [14]. This effect occurs due to the reduction in intermolecular forces within the polymer chains as the temperature rises. The increased thermal energy disrupts the regular packing of polymer chains, leading to increased chain mobility and reduced resistance to deformation [15]. High strain rate also causes changes in the yielding and plastic flow behaviour resulting in a continuous hardening and loss in ductility [16–20]. Finally, composite components used in aerospace structures are

* Corresponding author.
E-mail address: g.quino-quispe@imperial.ac.uk (G. Quino).

https://doi.org/10.1016/j.ijmecsci.2025.110683
Received 5 March 2025; Received in revised form 17 July 2025; Accepted 30 July 2025
Available online 31 July 2025
0020-7403/© 2025 The Author(s). Published by Elsevier Ltd. This is an open access article under the CC BY license (http://creativecommons.org/licenses/by/4.0/).

subjected to a broad range of temperatures during their service life. In particular, the temperature of an aircraft operating at cruise altitude is approximately −55 °C. It has been reported that thermoplastic materials exposed to progressively lower temperatures undergo a transition known as the ductile-to-brittle transition. This effect occurs due to the decreased mobility of polymer chains as the temperature drops. The reduced thermal energy restricts the movement of polymer chains, leading to diminished chain flexibility and increased intermolecular interactions. Consequently, PEEK becomes more rigid and prone to brittle fracturing when subjected to loads [21]. The mismatch of the thermal expansion coefficient between the fibres and the matrix also results in internal stresses, with a pronounced effect on the strength of the composites [22].

It is not sufficient to know only the effect of strain rate on stiffness and strength properties of the fibre reinforced composites as there is a significant effect on the energy absorption, crack propagation mechanisms, and failure modes of composite materials. The characterization of fracture behaviour under dynamic loading conditions is critical for the adoption of composite materials in high performance structural applications. The fracture toughness of composites can be classified into interlaminar, intralaminar and translaminar fracture [23]. Translaminar failure occurs when the crack propagates through the thickness of the laminate [24,25]. The translaminar fracture toughness not only plays an important role in the assessment of the damage tolerance of composite structures and their behaviour during damage propagation, but it is also relevant in the definition of the softening laws required in predictive numerical models [26]. Under tension, fracture usually occurs as a result of fibre breakage and pull-out, while under compression, this process is through crushing or kinking. It has been reported that a significant fraction of the impact energy is dissipated by creating the translaminar fracture surface and therefore it is essential to investigate the strain rate effects of translaminar fracture [27]. However, there is no consensus on the influence of strain rate on the translaminar fracture with different research publications indicating contradictory results depending on specimen geometry and data reduction methods [28]. Temperature is another factor that can influence the capability of composites to resist crack growth. At subzero temperatures, it has been reported that embrittlement of the matrix causes a reduction in fracture toughness of composites [29]. Similarly, at elevated temperatures fibre bridging and matrix ductility can cause increase in fracture toughness [25]. It is therefore recommended to test the mechanical behaviour of aerospace composites at different temperatures (−55 °C, 20 °C and 90 °C) pertinent to the service life of aerospace structures [30].

The strain energy release rate (SERR) can be determined by measuring the applied load and crack length during crack propagation, and then using fracture mechanics principles. There is considerable literature about the interlaminar failure of carbon fibre composites but there is limited data on fracture energy due to fibre failure [31,32]. Translaminar fracture, mainly dominated by fibre failure, requires more energy compared to matrix driven failure processes [33,34]. Experimental determination of the fracture toughness associated with these fibre failure modes is significant to accurately model the fibre-dominated damage behaviour. Compact Compression (CC) and Compact Tension (CT) tests originally designed for the testing of metallic materials have been adapted for the determination of both tensile and compressive fibre-dominated fracture toughness [35]. Other researchers such as Catalanotti et al. [36] used similar configuration of CT test of thermoset composites and applied Digital Image Correlation (DIC) technique for identification of the crack tip location to characterize the crack resistance curve (*R*-curve). The strain energy release rate (*G*) can be evaluated via several techniques. Common methods include the compliance method, experimental compliance calibration, the area method, or finite element analysis [37]. It was reported that analysing the propagation of translaminar cracks presents challenges because longitudinal fractures and delamination resulting from matrix cracking and fibre/matrix debonding tend to happen simultaneously with fibre fracture [38]. The choice of the testing configuration can significantly impact the measurement of fracture toughness, and this may be influenced by factors such as specimen specifications (including matrix type, fibre orientation, and stacking sequence), the dominance of delamination mechanics, the stress concentration near the crack tip, and other failure mechanisms occurring in regions opposite to the crack tip [39].

This paper investigates the combined effect of high strain rate and temperature on the critical translaminar strain energy release rate of fibre fracture in tension of CF/PEEK composites. Dynamic compact tension experiments are conducted at high loading rates using a Split Hopkinson Pressure Bar (SHPB). Additionally, the effect of temperature on the fracture properties is investigated by conducting the tests at room, hot (90 °C), and cold (−55 °C) temperatures.

In the following section, the material, specimen design, and experimental techniques are described. Section 3 presents and discusses the results, including the mechanical tests and post-mortem analysis using SEM and micro computed tomography (micro-CT) scans. Finally, Section 4 provides concluding remarks.

2. Experimental

2.1. Material and specimen manufacture

The compact tension specimen design and layup were based on those introduced by Pinho and Laffan [40–42]. Originally developed to characterise the translaminar fracture toughness of composites under quasi-static conditions, they have since been adapted for high-speed experiments by other authors [43–47].

A 305 mm × 305 mm composite plate with 34 plies, with a layup $[(90°, 0°)_8, 90°]_s$, was made of AS4/PEEK APC2 thermoplastic prepreg supplied by Solvay with a weight fraction of resin of 34 %. The plate was manufactured in a hot press, where it was consolidated at a temperature of 390 °C for 20 min under a prescribed total force of 62 kN, following the cycle recommended by the supplier. Specimens were cut from this plate with water jet and finely grounded to the final geometry (except the 10 mm cut) shown in Fig. 1. The sharp notch was created in two steps: (i) a 10 mm straight cut was made using a low-speed precision sectioning saw (IsoMet 5LC, Buehler, USA); and (ii) a 0.1 mm micro saw ('micro dozuki') was used with a careful sawing motion to produce the final crack tip.

2.2. Mechanical characterisation

Quasi-static (QS) experiments were conducted in the screw-driven universal testing machine Zwick Z250 (Zwick, Germany) with a pre-

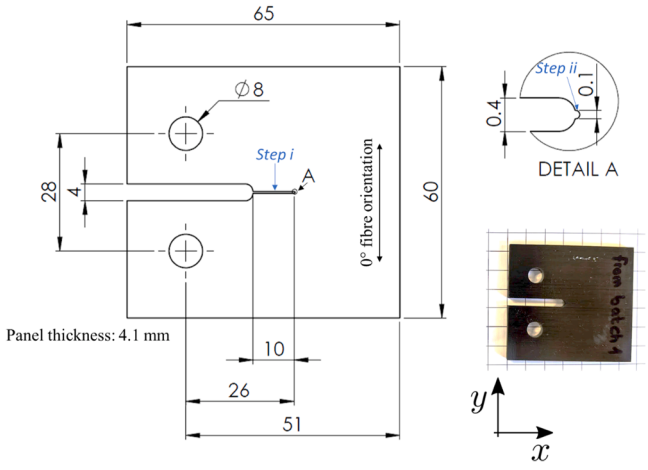


Fig. 1. Compact tension specimen design, showing dimensions and indicating the two steps to produce the crack tip.

scribed crosshead speed of 0.5 mm/min. The load was applied in the *y*-direction (see Fig. 1) via cylindrical loading pins of 8 mm diameter. A camera BM-500GE (JAI Ltd, Japan) was setup to capture 1 photograph per second at a resolution of 2456 × 2058 pixels. The applied load was measured with a 20 kN load cell mounted in the machine's crosshead. The history of opening displacement (*OD*) was measured using DIC to track the loading pins.

Dynamic impact or high-rate (HR) tests were conducted in the tensile split-Hopkinson pressure bar (Fig. 2) developed by Gerlach et al. [48]; further details about this configuration can be found in the original publication. Titanium bars with a solid circular cross-section of 16 mm diameter were used. In this apparatus, a 3.6 m loading bar was impacted by a striker with a U-shaped cross section, generating a tensile stress wave that travelled through the input bar, the specimen and the output bar. A 2.5 m long striker was used to achieve a long-duration stress pulse, necessary to trigger sufficient crack extension for reliable *R*-curve measurements. The input and output bars were instrumented, respectively, with two and one sets of strain gauges (SG) in half bridge configuration. The history of forces acting upon the specimen was calculated via one-dimensional wave propagation analysis and the voltage signals obtained from the three sets of strain gauges, following the procedure described in reference [49]. Images were acquired with the ultra-high-speed camera Kirana (Specialised Imaging, UK) at a rate of 250,000 frames per second, and a resolution of 924 × 768 pixels, with 0.63 mm/pixel. This camera could only capture up to 180 images per experiment. The history of opening displacement (*OD*) in high-rate tests was obtained with Digital Image Correlation analysis (DIC), tracking speckled surfaces rigidly attached to the loading pins (see detail in Fig. 2). The opening speeds in our experiments ranged from 4 m/s to 5 m/s which would correspond to expected strain rates in the order of tens of s^{-1}, as shown by Hoffmann *et al.* using their reference length approach [31].

Four testing scenarios were considered in this experimental campaign: the baseline case of Quasi-static at room temperature (QS/RT), high-rate at room temperature (HR/RT), high-rate at +93 °C (HR/Hot) and high-rate at −55 °C (HR/Cold). The temperature was prescribed with an environmental chamber that circulates preconditioned air at the required temperature, also used in previous studies [50]. The chosen hot and cold temperatures corresponded to the range of in-service temperatures that aircrafts may encounter [30,51,52].

All specimens were prepared with black speckle on white background using the "tattoo" speckle, allowing to produce optimal speckle sizes and distributions [53]. The resulting speckle sizes in the quasi-static and high-speed image series were approximately 4 pixels and 3 pixels respectively, matching recommendations for good speckle sizes in the literature [53–55]. All DIC analysis was conducted using the software LaVision Davis v. 10.1.2 using "relative to first" algorithm, and right Cauchy strain formulation.

In both quasi-static and high-rate experiments, the history of crack growth Δa was calculated via an in-house algorithm that handled the full-field *y*-direction strain components ε_y obtained by DIC. We used a threshold ε_y^{th} on the *y*-direction strain components to identify the real position of the crack tip. Similar strategies have been previously proposed and successfully used by other researchers [56–58]. The threshold ε_y^{th} was chosen to be 1.5 %, following the analysis of the field of shear strains. The selected $\varepsilon_y^{th} = 1.5\%$ was consistently right in between the positive and negative fields of shear strains as expected from the analytical solutions of the strain fields around the crack tip [59]. The threshold was the same for all testing conditions, as this failure mode is mainly driven by fibre breakage. Literature reports tensile strains to failure of carbon fibre composites to be independent of strain rate and temperature [60] . The value of the selected threshold is also consistent with strains to failure in longitudinal tension of thermoplastic composites [61].

2.3. Data reduction method

The critical energy release rate was calculated with the area method as in reference [31]. In this method, we assume that the fracture energy is primarily released in the breakage of fibres within the zero-degree plies, aligned with the loading direction *y* (see Fig. 1). This method has been reported to produce results like those obtained using the compliance method [45].

From the load (*P*) *vs.* opening displacement (*OD*) curve shown in Fig. 3, the area defined by the loading curve and the origin represent the energy ΔU that was released to advance the crack by Δa (crack growth). Under this assumption, the critical energy release rate of the laminate

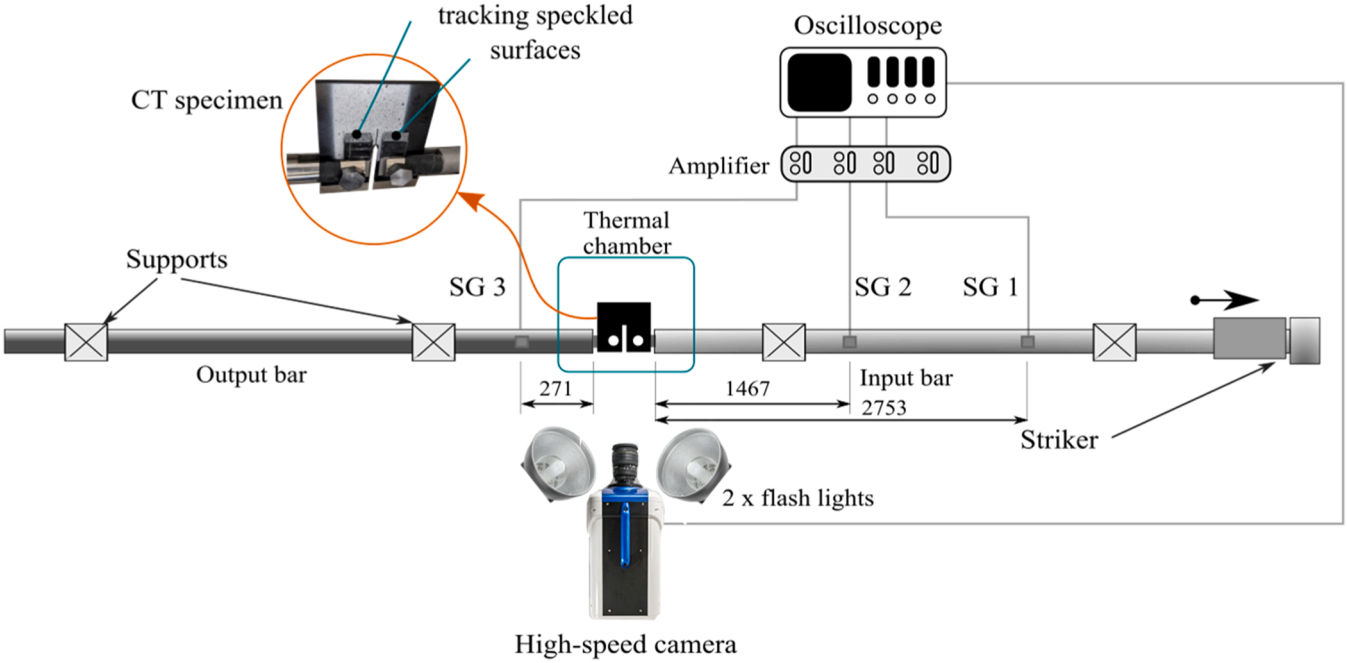


Fig. 2. Experimental setup for the high-speed compact tension experiments using a tensile split-Hopkinson pressure bar.

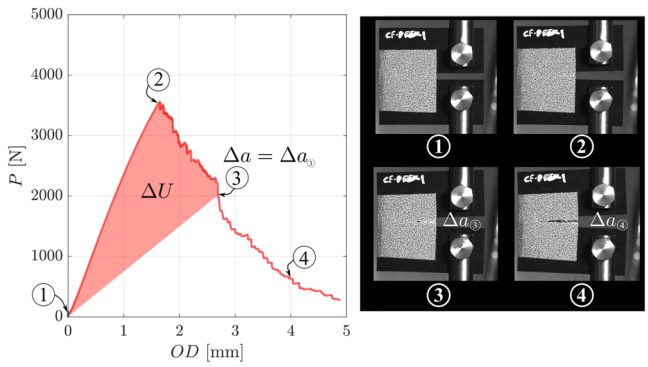


Fig. 3. The area method on a typical curve Force (*P*) *vs*. Opening Displacement (*OD*) to evaluate the critical translaminar energy release rate.

G_{Ic}^{lam} can be calculated with Eq. (1):

$$G_{Ic}^{lam}(\Delta a) = \frac{1}{2t_{lam}\Delta a}\Delta U, \tag{1}$$

where t_{lam} is the thickness of the laminate (~4.1 mm), Δa is the crack growth. The energy ΔU can be evaluated numerically using the data points from the *OD vs. P* plot.

We assume that practically all the fracture energy is released by fibre breakage in the plies oriented at 0° degrees. Therefore, the mode-I translaminar critical energy release rate G_{Ic}^{f+} can be calculated as:

$$G_{Ic}^{f+} = \frac{t_{lam}}{t_0}G_{Ic}^{lam}, \tag{2}$$

where t_0 is the total thickness of all 0° plies.

2.4. Scanning electron microscopy and micro computed tomography

Post-mortem imaging of the fracture surfaces for all testing cases was conducted using SEM, in the tabletop microscope TM3030Plus (Hitachi, Japan) using the BSE detector and 15 kV accelerating voltage. The internal damage of quasi-static and high-rate specimens was assessed via x-Ray micro computed tomography with a custom Nikon XTEK XTH 225 kVp micro-focus CT system at Mu-Vis X-ray Imaging Centre, Southampton with a resolution of 10.4 µm. The 3D volume was reconstructed from 3000 projections that were captured as the samples were rotated by 360° Each projection image was saved in a 2000 px by 2000 px, 16 bits depth image file.

3. Results and discussion

Typical *P vs. OD* curves at quasi-static and high-rate tests are shown in Fig. 4a. In both quasi-static and dynamic regimes, as *OD* increases, the force displays an initial linear rise up to a point of maximum load P_m, followed by a gradual load decrease because of the propagating crack and other occurring damage mechanisms. Stable crack progression was observed in the quasi-static regime, in contrast to the stick-slip crack propagation reported on thermoset composites [41,43]. At high-rate, the stiffness of the specimen seems to be greater than under quasi-static loading, in agreement with what Hoffmann *et al.* observed in their experiments [43]. This should be taken with care, because from the nature of Hopkinson bar experimentation, the initial part of the loading curve corresponds to a region without dynamic equilibrium, and the load measurements may not be reliable. However, dynamic disequilibrium, defined as how distinct the loads on opposite sides of the specimen are [43,62], was sufficiently low before P_m was reached, as shown in [43], thereby allowing us to draw general conclusions.

Fig. 4b shows the influence of temperature upon the *P vs. OD* curves at high-rate. The slopes of the initial "linear" loading regions seem to be nearly the same across all temperatures. Therefore, for the ranges of temperatures and loading rate herein considered, the apparent stiffness of the specimens is not significantly affected. In this loading direction, the stiffness of the specimen is mainly dominated by the stiffness of the 0° plies, which seem to be unaffected by the temperature. This is in line with the observations of the temperature dependency of elastic moduli of carbon fibre and CFRPs reported in the literature [63,64].

A summary of the maximum load P_m for all cases is shown in Fig. 5. From quasi-static to high-rate, P_m increases by 40 %. In the dynamic regime, at 90 °C, P_m is 9 % lower than at room temperature RT, possibly due to matrix plasticisation and interface weakening caused by elevated temperatures [11], which reduces its capability to redistribute loads. This can be associated to the reduction in longitudinal tensile strength with increasing temperature, previously observed in quasi-static experiments [65,66]. At −55 °C, P_m is not significantly different than the maximum load at HR/RT, suggesting that the system is almost insensitive to lower temperatures.

Fig. 6 shows the sensitivity of the resulting history of crack growth Δa to the choice of ε_y^{th} threshold in the range 1 % to 10 % for QS and HR

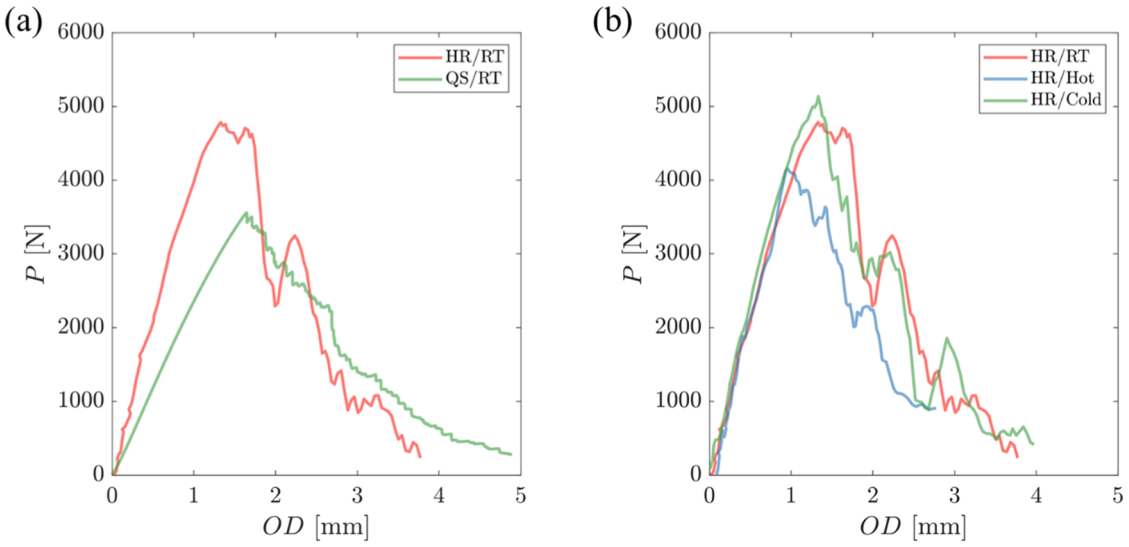


Fig. 4. Comparison of representative Load (*P*) *vs.* Opening Displacement (*OD*) at (a) quasi-static and dynamic regimes at room temperature and (b) across various temperatures in the dynamic regime.

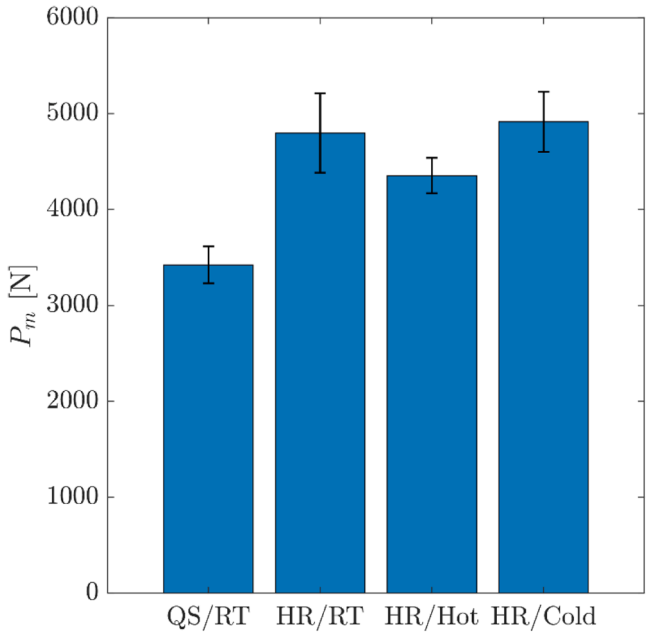


Fig. 5. Average and standard deviations of the maximum loads P_m measured across all tests.

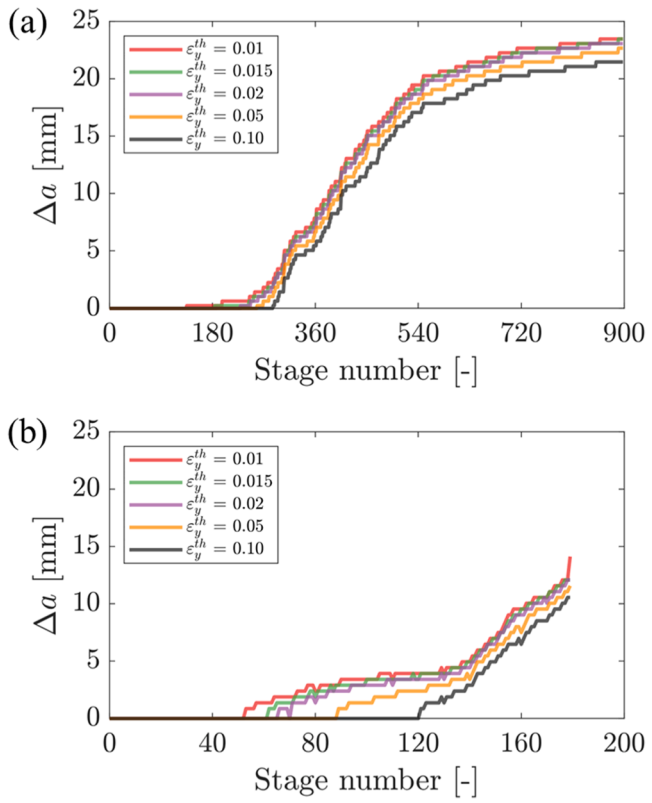


Fig. 6. Sensitivity of the measured crack growth history with respect to the selected strain threshold ε_y^{th} in representative (a) quasi-static, and (b) high-rate experiments.

experiments. The parametric analysis shows that high-rate results would be more sensitive to the selection of a threshold value, given our data reduction methodology. This could be due to the high speed of the crack propagation as well as the typically lower quality high-speed images, with smaller resolution and bit depth. The results also show that for the chosen threshold of 1.5 % and within a variability of ±0.5%, the resulting history of crack growth would not change significantly.

Fig. 7 shows a representative set of curves for the histories of load, opening displacement and crack growth, for a quasi-static experiment, resulting from the data reduction procedure described above (Section 2.3). Using these histories corresponding to each experiment, and Eq. (2), the resulting *R*-curves for all experiments are presented in Fig. 8.

Taking the average of the values within the "plateau" section of the *R*-curves, for $\Delta a > 5$ mm, we calculated representative average values of the propagation critical mode-I translaminar energy release rates, summarised in Fig. 9. The quasi-static value of $G_{Ic}^{f+} = 171.8 \pm 3.2$ kJ/m^2 falls within the range of values reported in the literature, summarised by Monticeli *et al.* [67]. From quasi-static to high-rate at room temperature, the translaminar critical energy release rate increased by about 20 %. This is in line with the increase of fracture toughness with loading rate reported in [68–70], but opposite to the trends reported in [43,45]. There is certainly disagreement in the trends reported in literature for the dependency of translaminar fracture toughness with loading rate, possibly owing to the distinct experimental characterisation and data reduction methods.

Within the dynamic regime, from HR/RT to HR/Hot, G_{Ic}^{f+} drops by 27 %. This could be due to the temperature weakening the matrix and interfaces that reduce the amount of energy being dissipated during fracture. However, by comparing HR/RT and HR/Cold, the translaminar energy release rate seems to be unaffected, a similar neutral effect to what it was observed with the maximum load P_m.

Fig. 10 shows the side views of the fracture surfaces for all the testing cases. One of the main energy dissipation mechanisms in translaminar failure is fibre pullout, which can be observed with higher detail in the SEM microscopies shown in Figs. 11, 13 and 14. Fibre pullout lengths and their distribution have been previously linked to the measured fracture toughness [41,71–73]. In general, longer fibre pullouts were found to correlate with higher measured translaminar fracture toughness. In Figs. 10 and 11, when comparing QS/RT and HR/RT fracture surfaces, the high-rate specimens showed longer pullout lengths, which suggests that the frictional fibre pullout forces contributed with higher amount of work done, therefore leading to higher measured fracture energies, aligning with the experimental observations.

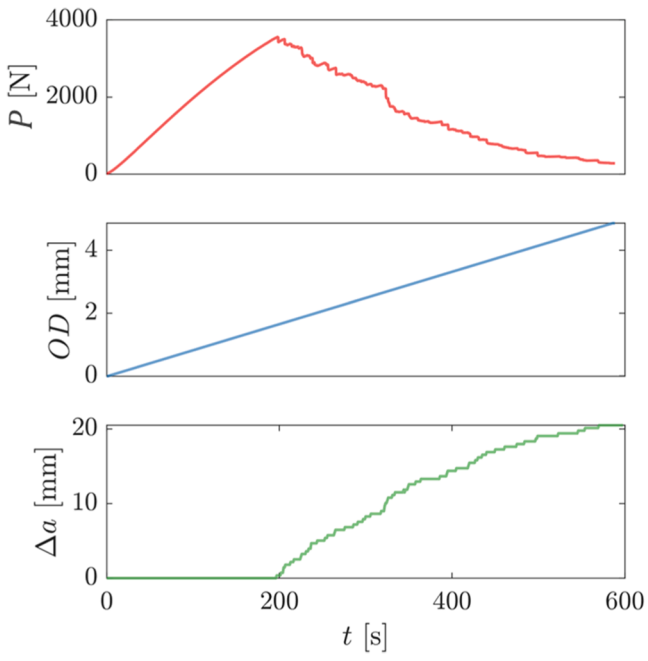


Fig. 7. Histories of load (*P*), opening displacement (*OD*), and crack growth (Δa) in a representative quasi-static experiment.

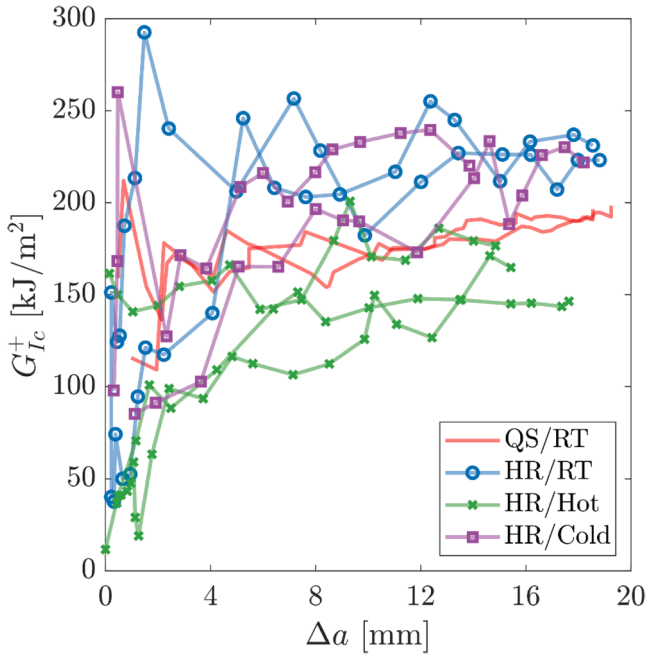


Fig. 8. *R*-curves showing critical energy release rates G_{Ic}^{f+} for all testing scenarios.

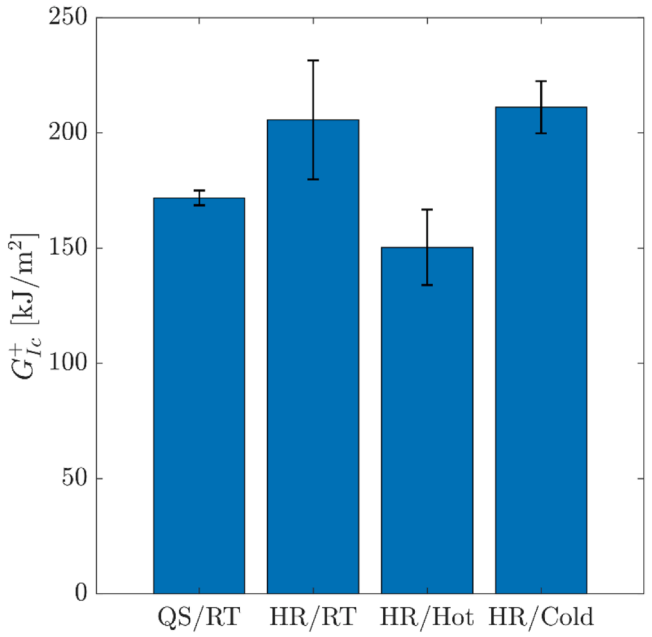


Fig. 9. Average critical energy release rates G_{Ic}^{f+} for all testing cases.

Fig. 12 shows the X-ray computer tomography images of representative QS/RT and HR/RT fractured samples. In addition to fibre pullouts, multiple intralaminar or transverse cracks can be observed within the 90° layers. This intralaminar cracking is significantly more prevalent in the specimen tested at high rate than in the quasi-static specimen, therefore contributing to the higher measured fracture energy. The embrittlement of the transverse tensile response, and consequent reduction in transverse strain to failure at higher strain rates, may be responsible for this higher number of transverse cracks.

Figs. 13 and 14 show the fracture surfaces of specimens HR/Hot and HR/Cold, tested at high rate, but at elevated and low temperatures, respectively. The SEM images do not show a clear difference in terms of

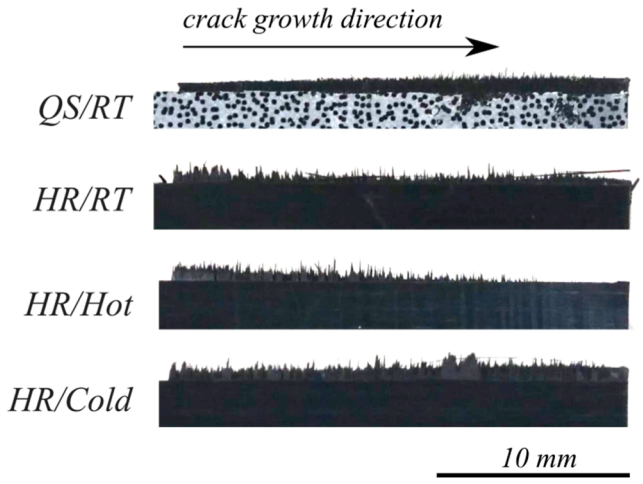


Fig. 10. Side view of fracture surfaces of compact tension specimens tested at different loading rates and temperatures.

pullout lengths. However, as shown in Fig. 9, there is a notable difference in their fracture energy.

We also used DIC to assess the extension of damage, as previously done by other researchers [43,54]. Fig. 15 shows the full ε_y strain field during the HR/Hot and HR/Cold experiments. In both cases, the selected frames correspond to an instant where both specimens have the same crack growth $\Delta a = 10$ mm. The region with higher strains is larger in the HR/Cold specimen, suggesting more diffused damage taking place at low temperatures. Additionally, HR/Cold specimens displayed multiple intralaminar cracking in the 90° outer layers (Fig. 15), which likely contributed to additional energy dissipation.

It is worth noting that the lower critical strain energy release rate was for higher temperature in the high-rate experiments. This is contrary to the trend reported by Yu *et al.* for the quasi-static translaminar fracture toughness of epoxy/carbon fibre composites [51]. It can be hypothesised that the reason for this reversal is the smaller contribution of the pullout frictional stress at high rates. Yu et al. [51] proposed an analytical model relating the pullout frictional stress and interfacial shear strength, and the translaminar fracture toughness and showed that the trend of increasing translaminar fracture toughness with higher temperatures based on the composite's interfacial properties. However, when the frictional stresses are small, their map suggests an opposite trend. It is reasonable to assume that during high-rate loading, the frictional contribution becomes less relevant due to the dynamic nature of the event. The pullout stresses at high-rate being small enough, their model would suggest that the higher temperatures will result in lower fracture energy. However, the required interfacial data does not exist at high-rate, and more work is required to explain the dependency of the strain rate and temperature on translaminar toughness.

4. Conclusions

This study investigated the combined effect of strain rate and temperature on the translaminar critical strain energy release rate G_{Ic}^{f+} of CF/PEEK composites. Dynamic compact tension experiments were conducted using a Split Hopkinson Pressure Bar (SHPB) to evaluate the critical translaminar strain energy release rate under high loading rates. The experimental results demonstrated the strain rate dependency of translaminar fracture toughness by comparing quasi-static and high-rate loading at room temperature. Additionally, the influence of temperature was assessed by performing tests at room temperature, elevated temperature (90 °C), and subzero temperature (−55 °C) in the dynamic regime, which owing to the experimental challenges involved has been rarely studied. Postmortem analysis with SEM and X-ray micro-CT were

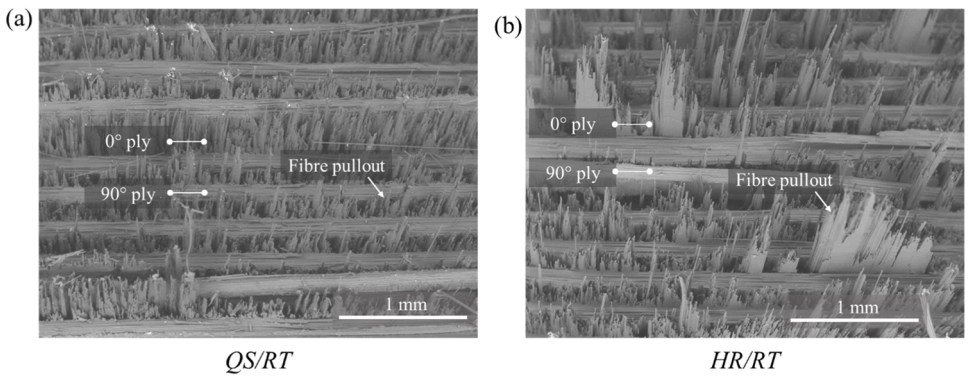


Fig. 11. SEM micrography images of the fracture surfaces of specimens tested at room temperature under (a) quasi-static, and (b) high-rate loading conditions.

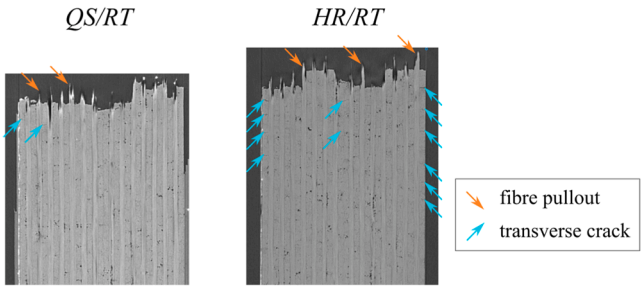


Fig. 12. Micro-CT images of QS/RT and HR/RT specimens showing fibre pullouts and transverse cracks.

also conducted, obtaining relevant clues on the damage mechanisms driving this type of fracture. The main conclusions of this study are:

- The use of Digital Image Correlation (DIC) in both quasi-static and high-rate tests has proven effective in tracking crack growth with high precision. The ε_y threshold method enabled consistent crack tip identification across all testing conditions, demonstrating the robustness of this approach for fibre-dominated failure analysis.
- At high strain rates, increasing the temperature to 90 °C resulted in a significant reduction in fracture toughness, likely due to matrix softening and interface weakening. DIC analysis show smaller damaged regions, in line with their lower measured critical strain energy release rate.
- Conversely, lowering the temperature to −55 °C did not significantly affect the fracture toughness, suggesting that temperature-induced embrittlement was not the dominant failure mechanism under these conditions.

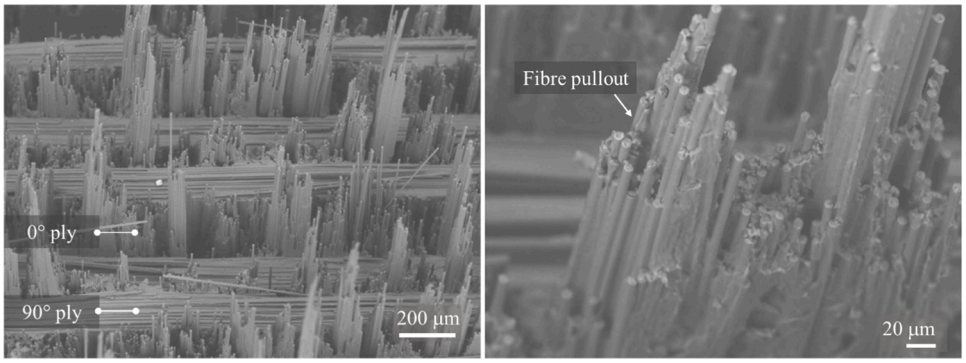


Fig. 13. SEM micrography images of the fracture surfaces of HR/Hot specimens.

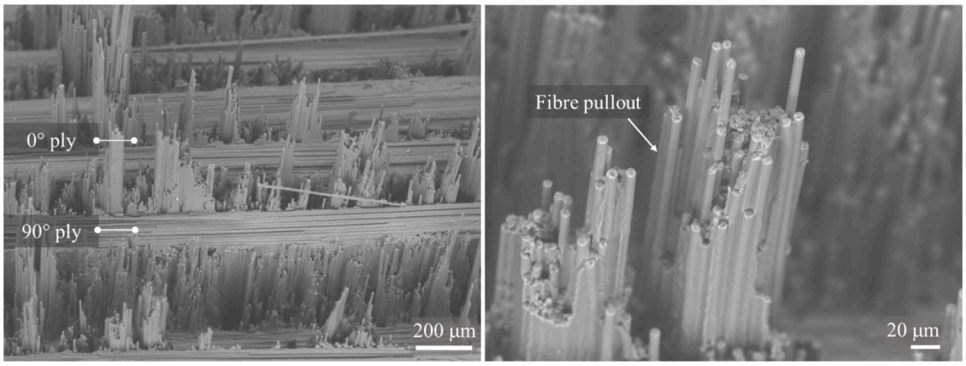


Fig. 14. SEM micrography images of the fracture surfaces of HR/Cold specimens.

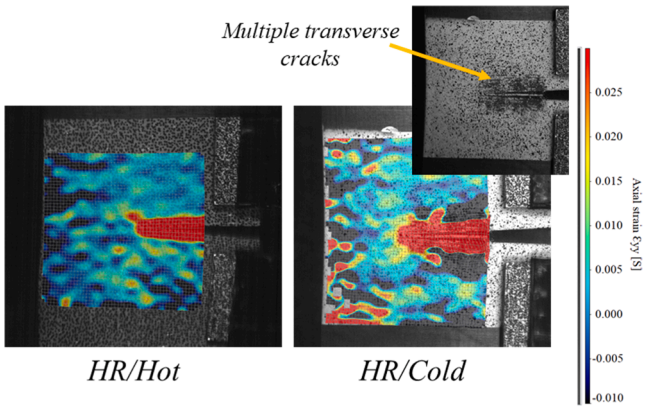


Fig. 15. DIC full strain fields showing the levels of diffused damaged at different temperatures.

- The pullout lengths showed strong correlation with measured fracture toughness at room temperature when comparing QS/RT to HR/RT.
- Transverse cracking seemed to be an additional failure mechanism arising at high loading rate at different temperatures.

The findings highlight the necessity of testing CF/PEEK composites under service-relevant conditions, including extreme temperatures and high strain rates, to ensure reliable performance in aerospace applications. Future work should focus on quantifying interfacial properties at high strain rates and temperatures to develop more accurate constitutive models for high-performance composite structures.

CRediT authorship contribution statement

Gustavo Quino: Writing – review & editing, Writing – original draft, Visualization, Software, Project administration, Methodology, Investigation, Formal analysis, Data curation, Conceptualization. **Karthik Ram Ramakrishnan:** Writing – review & editing, Writing – original draft, Supervision, Resources, Project administration, Methodology, Investigation, Formal analysis, Conceptualization.

Declaration of competing interest

The authors declare that they have no known competing financial interests or personal relationships that could have appeared to influence the work reported in this paper.

Acknowledgements

The authors would like to thank Solvay for supplying the thermoplastic prepreg material; and Dr Tomas Katafiasz from Imperial College London for his generous help in manufacturing the composite panel. We would also like to thank the Impact Engineering Lab at the University of Oxford, and Dr Antonio Pellegrino for kindly supporting our affiliations as visiting researchers. Finally, we acknowledge the support of Mu-VIS X-Ray Imaging Centre for facilitating the micro-CT scans.

For the purpose of open access, the author has applied a Creative Commons Attribution (CC BY) licence to any Author Accepted Manuscript version arising.

Data availability

Data will be made available on request.

References

[1] Ozturk F, Cobanoglu M, Ece RE. Recent advancements in thermoplastic composite materials in aerospace industry. J Thermoplast Compos Mater 2023;37(9):3084–116. https://doi.org/10.1177/08927057231222820.
[2] Andrew JJ, Ubaid J, Cantwell WJ, Khan KA, Umer R. The effect of cryogenic thermal cycling on impact performance of graphene-enhanced recyclable liquid thermoplastic/carbon fiber composites for hydrogen storage applications. Compos C Open Access 2025;17:100601. https://doi.org/10.1016/J.JCOMC.2025.100601. Jul.
[3] Hou W, He P, Yang Y, Sang L. Crashworthiness optimization of crash box with 3D-printed lattice structures. Int J Mech Sci 2023;247:108198. https://doi.org/10.1016/J.IJMECSCI.2023.108198. Jun.
[4] Hu J, et al. Two-position impact behavior and interference mechanism of CFF/PEEK thermoplastic composites. Int J Mech Sci 2022;232:107644. https://doi.org/10.1016/J.IJMECSCI.2022.107644. Oct.
[5] Touchard F, Lafarie-Frenot MC, Guédra-Degeorges D. Mechanical behaviour characteristics of a thermoplastic composite used in structural components. Compos Sci Technol 1996;56(7):785–91. https://doi.org/10.1016/0266-3538(96)00021-8.
[6] Yao SS, Jin FL, Rhee KY, Hui D, Park SJ. Recent advances in carbon-fiber-reinforced thermoplastic composites: a review. Compos B Eng 2018;142:241–50. https://doi.org/10.1016/j.compositesb.2017.12.007. December 2017.
[7] Zhang J, et al. The effect of cooling rates on crystallization and low-velocity impact behaviour of carbon fibre reinforced poly(aryl ether ketone) composites. Compos B Eng 2023;254:110569. https://doi.org/10.1016/j.compositesb.2023.110569. February.
[8] Zomer D, Simaafrookhteh S, Vanclooster K, Dorigato A, Ivens J. Forming-behavior characterization of cross-ply carbon fiber/PA6 laminates using the bias-extension test. Compos Appl Sci Manuf 2023;168:107436. https://doi.org/10.1016/j.compositesa.2023.107436. September 2022.
[9] Kawai M, Masuko Y, Kawase Y, Negishi R. Micromechanical analysis of the off-axis rate-dependent inelastic behavior of unidirectional AS4/PEEK at high temperature. Int J Mech Sci 2001;43(9):2069–90. https://doi.org/10.1016/S0020-7403(01)00029-7. Sep.
[10] Daniel J, Gonzalez P, Bouvet C, Vieille B. Translaminar cracking modeling in woven ply thermoplastic laminates in tension and in compression. Appl Compos Mater 2023;(0123456789). https://doi.org/10.1007/s10443-023-10128-6.
[11] Zhang Y, Sun L, Li L, Wei J. Effects of strain rate and high temperature environment on the mechanical performance of carbon fiber reinforced thermoplastic composites fabricated by hot press molding. Compos Appl Sci Manuf 2020;134:105905. https://doi.org/10.1016/J.COMPOSITESA.2020.105905. Jul.
[12] Perry JI, Walley SM. Measuring the effect of strain rate on deformation and damage in fibre-reinforced composites: a review. J Dyn Behav Mater 2022;8(2):178–213. https://doi.org/10.1007/s40870-022-00331-0.
[13] El-Qoubaa Z, Othman R. Tensile behavior of polyetheretherketone over a wide range of strain rates. Int J Polym Sci 2015;2015. https://doi.org/10.1155/2015/275937.
[14] Pan Z, Yang C, Huang S, Wang M, Wu Z, Gu B. High strain-rate compression behavior of woven CF/PEEK thermoplastic composites at the glassy state and high-elastic state. Int J Mech Sci 2022;235:107740. https://doi.org/10.1016/J.IJMECSCI.2022.107740. Dec.
[15] Barba D, Arias A, Garcia-Gonzalez D. Temperature and strain rate dependences on hardening and softening behaviours in semi-crystalline polymers: application to PEEK. Int J Solids Struct 2020;182–183:205–17. https://doi.org/10.1016/j.ijsolstr.2019.08.021.
[16] El-Qoubaa Z, Othman R. Characterization and modeling of the strain rate sensitivity of polyetheretherketone's compressive yield stress. Mater Des 2015;66:336–45. https://doi.org/10.1016/j.matdes.2014.10.080. PA.
[17] Thomson D, Quino G, Cui H, Pellegrino A, Erice B, Petrinic N. Strain-rate and off-axis loading effects on the fibre compression strength of CFRP laminates: experiments and constitutive modelling. Compos Sci Technol 2020;195:108210. https://doi.org/10.1016/j.compscitech.2020.108210. Jul.
[18] El-Qoubaa Z, Othman R. Tensile behavior of polyetheretherketone over a wide range of strain rates. Int J Polym Sci 2015;2015. https://doi.org/10.1155/2015/275937.
[19] Chen C, Zhang C, Zhao Z, Wang Y, Wong SC, Li Y. Effect of fiber reinforcement and fabrication process on the dynamic compressive behavior of PEEK composites. Int J Mech Sci 2019;155:170–7. https://doi.org/10.1016/J.IJMECSCI.2019.02.034. May.
[20] Quino G, Pellegrino A, Tagarielli VL, Petrinic N. Measurements of the effects of pure and salt water absorption on the rate-dependent response of an epoxy matrix. Compos B Eng 2018;146:213–21. https://doi.org/10.1016/j.compositesb.2018.03.044. Aug.
[21] Garcia-Gonzalez D, Rodriguez-Millan M, Rusinek A, Arias A. Low temperature effect on impact energy absorption capability of PEEK composites. Compos Struct 2015;134:440–9. https://doi.org/10.1016/j.compstruct.2015.08.090. Dec.
[22] Tang Z, Chen C, Li A, Deng Y, Zhang C, Li Y. Temperature- and strain-rate-dependent tensile failure behavior of short-fiber-reinforced PEEK composites. Compos B Eng 2023;250:110455. https://doi.org/10.1016/j.compositesb.2022.110455. July 2022.
[23] Laffan MJ, Pinho ST, Robinson P, McMillan AJ. Translaminar fracture toughness testing of composites: a review. Polym Test 2012;31(3):481–9. https://doi.org/10.1016/j.polymertesting.2012.01.002.

[24] Laffan MJ, Pinho ST, Robinson P, McMillan AJ. Translaminar fracture toughness testing of composites: a review. Polym Test 2012;31(3):481–9. https://doi.org/10.1016/J.POLYMERTESTING.2012.01.002. May.
[25] Zeinedini A, Hasan YB. Effect of temperature on the mixed mode I/II translaminar fracture of epoxy composites reinforced with cotton fibers. Appl Compos Mater 2024;32(1):281–302. https://doi.org/10.1007/S10443-024-10267-4/FIGURES/15. Feb.
[26] Kuhn P, Catalanotti G, Xavier J, Ploeckl M, Koerber H. Determination of the crack resistance curve for intralaminar fiber tensile failure mode in polymer composites under high rate loading. Compos Struct 2018;204:276–87. https://doi.org/10.1016/J.COMPSTRUCT.2018.07.039. Nov.
[27] Swolfs Y, Geboes Y, Gorbatikh L, Pinho ST. The importance of translaminar fracture toughness for the penetration impact behaviour of woven carbon/glass hybrid composites. Compos Appl Sci Manuf 2017;103:1–8. https://doi.org/10.1016/j.compositesa.2017.09.009.
[28] Thomson D, et al. A review of the effect of loading rate on the mechanical properties of unidirectional carbon fibre reinforced polymer composites. Compos Appl Sci Manuf 2025:108773. https://doi.org/10.1016/J.COMPOSITESA.2025.108773. Feb.
[29] Machado JJM, Marques EAS, Campilho RDSG, da Silva LFM. Mode I fracture toughness of CFRP as a function of temperature and strain rate. J Compos Mater 2017;51(23):3315–26. https://doi.org/10.1177/0021998316682309.
[30] Katafiasz TJ, Greenhalgh ES, Allegri G, Pinho ST, Robinson P. The influence of temperature and moisture on the mode I fracture toughness and associated fracture morphology of a highly toughened aerospace CFRP. Compos Appl Sci Manuf 2021;142:106241. https://doi.org/10.1016/j.compositesa.2020.106241. Mar.
[31] Hoffmann J, Cui H, Petrinic N. Determination of the strain-energy release rate of a composite laminate under high-rate tensile deformation in fibre direction. Compos Sci Technol 2018;164:110–9. https://doi.org/10.1016/j.compscitech.2018.05.034. Aug.
[32] D. Ray et al., "Fracture toughness of carbon fiber /polyether ether ketone composites manufactured by autoclave and laser-assisted automated tape placement," vol. 41643, pp. 1–10, 2015, doi:10.1002/app.41643.
[33] Pimenta S, Pinho ST. An analytical model for the translaminar fracture toughness of fibre composites with stochastic quasi-fractal fracture surfaces. J Mech Phys Solids 2014;66:78–102. https://doi.org/10.1016/j.jmps.2014.02.001. May.
[34] Zeinedini A, Moradi MH, Taghibeigi H, Jamali J. On the mixed mode I/II/III translaminar fracture toughness of cotton/epoxy laminated composites. Theor Appl Fract Mech 2020;109:102760. https://doi.org/10.1016/J.TAFMEC.2020.102760. Oct.
[35] Pinho ST, Robinson P, Iannucci L. Fracture toughness of the tensile and compressive fibre failure modes in laminated composites. Compos Sci Technol 2006;66(13):2069–79. https://doi.org/10.1016/J.COMPSCITECH.2005.12.023. Oct.
[36] Catalanotti G, Camanho PP, Xavier J, Dávila CG, Marques AT. Measurement of resistance curves in the longitudinal failure of composites using digital image correlation. Compos Sci Technol 2010;70(13):1986–93. https://doi.org/10.1016/j.compscitech.2010.07.022.
[37] Laffan MJ, Pinho ST, Robinson P, Iannucci L. Measurement of the *in situ* ply fracture toughness associated with mode I fibre tensile failure in FRP. Part I: data reduction. Compos Sci Technol 2010;70(4):606–13. https://doi.org/10.1016/j.compscitech.2009.12.016.
[38] Monticeli FM, Fuga FR, Donadon MV. A systematic review on translaminar fracture damage propagation in fiber-reinforced polymer composites. Thin-Walled Struct 2023;187:110742. https://doi.org/10.1016/j.tws.2023.110742. March.
[39] Rutar R, Serra J, Bausiere Q, Bouvet C. Experimental characterization of tensile and compressive translaminar fracture toughness coupling multi-physics measurements. Eng Fract Mech 2023;291:109568. https://doi.org/10.1016/j.engfracmech.2023.109568. September.
[40] Pinho ST, Robinson P, Iannucci L. Fracture toughness of the tensile and compressive fibre failure modes in laminated composites. Compos Sci Technol 2006;66(13):2069–79. https://doi.org/10.1016/J.COMPSCITECH.2005.12.023. Oct.
[41] Laffan MJ, Pinho ST, Robinson P, Iannucci L. Measurement of the *in situ* ply fracture toughness associated with mode I fibre tensile failure in FRP. Part II: size and lay-up effects. Compos Sci Technol 2009;70:614–21. https://doi.org/10.1016/j.compscitech.2009.12.011.
[42] M.J. Laffan, S.T. Pinho, P. Robinson, and L. Iannucci, "Measurement of the *in situ* ply fracture toughness associated with mode I fibre tensile failure in FRP. Part I: data reduction," 2010, doi:10.1016/j.compscitech.2009.12.016.
[43] Hoffmann J, Cui H, Petrinic N. Determination of the strain-energy release rate of a composite laminate under high-rate tensile deformation in fibre direction. Compos Sci Technol 2018;164:110–9. https://doi.org/10.1016/j.compscitech.2018.05.034. Aug.
[44] Sommer DE, Thomson D, Hoffmann J, Petrinic N. Numerical modelling of quasi-static and dynamic compact tension tests for obtaining the translaminar fracture toughness of CFRP. Compos Sci Technol 2023;237:109997. https://doi.org/10.1016/j.compscitech.2023.109997. May.
[45] Cheng L, He R, Gao Y, Cui H, Li Y. Determination of fibre tension fracture toughness of composite laminates at high loading rate. Compos Sci Technol 2022;228:109619. https://doi.org/10.1016/j.compscitech.2022.109619. Sep.
[46] He R, Gao Y, Cheng L, Cui H, Li Y. Fracture toughness for longitudinal compression failure of laminated composites at high loading rate. Compos Appl Sci Manuf 2022;156:106834. https://doi.org/10.1016/J.COMPOSITESA.2022.106834. May.
[47] Yue Z, Shen X, Chang Z, Zou G. Effect of geometric parameters on dynamic fracture toughness of compact tensile specimens. Mech Based Des Struct Mach 2025;53(3):2116–34. https://doi.org/10.1080/15397734.2024.2402392.
[48] Gerlach R, Kettenbeil C, Petrinic N. A new split Hopkinson tensile bar design. Int J Impact Eng 2012;50:63–7. https://doi.org/10.1016/j.ijimpeng.2012.08.004. Dec.
[49] Quino G, Tagarielli VL, Petrinic N. Effects of water absorption on the mechanical properties of GFRPs. Compos Sci Technol 2020;199:108316. https://doi.org/10.1016/j.compscitech.2020.108316. Oct.
[50] Chen Y, Quino G, Pellegrino A. A comprehensive investigation on the temperature and strain rate dependent mechanical response of three polymeric syntactic foams for thermoforming and energy absorption applications. Polym Test 2024;130:108287. https://doi.org/10.1016/J.POLYMERTESTING.2023.108287. Jan.
[51] Yu B, et al. Hygrothermal effects on the translaminar fracture toughness of a highly toughened aerospace CFRP: experimental characterisation and model prediction. Compos Appl Sci Manuf 2021;150:106582. https://doi.org/10.1016/j.compositesa.2021.106582. Nov.
[52] Williams A, Hamerton I, Allegri G. Environmental effects of moisture and elevated temperatures on the mode I and mode II interlaminar fracture toughness of a toughened epoxy carbon fibre reinforced polymer. Polym (Basel) 2025;17(11):1503. https://doi.org/10.3390/POLYM17111503. *2025, Vol. 17, Page 1503*May.
[53] Quino G, et al. Speckle patterns for DIC in challenging scenarios: rapid application and impact endurance. Meas Sci Technol 2021;32(1):015203. https://doi.org/10.1088/1361-6501/abaae8. Jan.
[54] Quino G. Impact damage analysis of composite structures using digital image correlation. Non-destructive testing of impact damage in fiber-reinforced polymer composites. 2024. p. 69–86. https://doi.org/10.1016/B978-0-443-14120-1.00003-0. Jan.
[55] Sutton MA. Digital image correlation for shape and deformation measurements. In: Sharpe WN, editor. Springer handbook of experimental solid mechanics. Boston, MA: Springer US; 2008. p. 565–600. https://doi.org/10.1007/978-0-387-30877-7_20. ch. 20.
[56] P.L. Reu, B.R. Rogillio, and G.W. Wellman, "Crack tip growth measurement using digital image correlation," Jan. 01, 2007.
[57] A. Khudiakova, V. Grasser, C. Blumenthal, M. Wolfahrt, and G. Pinter, "Automated monitoring of the crack propagation in mode I testing of thermoplastic composites by means of digital image correlation," 2019, doi:10.1016/j.polymertesting.2019.106304.
[58] Mallon S, Koohbor B, Kidane A, Sutton MA. Fracture behavior of prestressed composites subjected to shock loading: a DIC-based study. Exp Mech 2015;55(1):211–25. https://doi.org/10.1007/s11340-014-9936-5.
[59] Anderson TL. FRACTURE MECHANICS: fundamentals and applications, fourth edition. Fracture mechanics: fundamentals and applications. 4th Edition 2017. p. 1–661. https://doi.org/10.1201/9781315370293/FRACTURE-MECHANICS-TED-ANDERSON/ACCESSIBILITY-INFORMATION. Jan.
[60] Gómez-del Río T, Barbero E, Zaera R, Navarro C. Dynamic tensile behaviour at low temperature of CFRP using a split Hopkinson pressure bar. Compos Sci Technol 2005;65(1):61–71. https://doi.org/10.1016/J.COMPSCITECH.2004.06.004. Jan.
[61] Ramaswamy K, Modi V, Rao PS, Martin PP, McCarthy CT, O'Higgins RM. An investigation of the influence of matrix properties and fibre–matrix interface behaviour on the mechanical performance of carbon fibre-reinforced PEKK and PEEK composites. Compos Appl Sci Manuf 2023;165:107359. https://doi.org/10.1016/J.COMPOSITESA.2022.107359. Feb.
[62] Ravichandran G, Subhash G. Critical appraisal of limiting strain rates for compression testing of ceramics in a split Hopkinson pressure bar. J Am Ceram Soc 1994;77(1):263–7. https://doi.org/10.1111/J.1151-2916.1994.TB06987.X.
[63] Sauder C, Lamon J, Pailler R. Thermomechanical properties of carbon fibres at high temperatures (up to 2000°C). Compos Sci Technol 2002;62(4):499–504. https://doi.org/10.1016/S0266-3538(01)00140-3. Mar.
[64] B.M. Walther, "An investigation of the tensile strength and stiffness of unidirectional polymer-matrix, carbon-Fiber composites under the influence of elevated temperatures," May 27, 1998. Accessed: Dec. 09, 2024. [Online]. Available: http://hdl.handle.net/10919/36803.
[65] Li Y, et al. Theoretical model for the temperature dependent longitudinal tensile strength of unidirectional fiber reinforced polymer composites. Compos B Eng 2019;161:121–7. https://doi.org/10.1016/j.compositesb.2018.10.056. Mar.
[66] Tsugiyuki O, Nakada M, Miyano Y. Temperature dependence of longitudinal tensile strength in unidirectional carbon fiber-reinforced plastic. J Compos Mater 2014;48(28):3569–73. https://doi.org/10.1177/0021998313512349/FORMAT/EPUB. Dec.
[67] Monticeli FM, Fuga FR, Donadon MV. A systematic review on translaminar fracture damage propagation in fiber-reinforced polymer composites. Thin-Walled Struct 2023;187:110742. https://doi.org/10.1016/j.tws.2023.110742. MarchJun.
[68] Moy P, Tzeng J. Loading rate effect on translaminar fracture toughness of hybrid composite laminate. In: *ASME International Mechanical Engineering Congress and Exposition, Proceedings (IMECE)*, vol. 2000–M; 2000. p. 79–85. https://doi.org/10.1115/IMECE2000-1960.
[69] Yoo S, Dalli D, Catalanotti G, Toso N, Kessel F, Voggenreiter H. Dynamic intralaminar fracture toughness characterisation of unidirectional carbon fibre-reinforced polymer composites using a high-speed servo-hydraulic test set-up. Compos Struct 2022;295:115838. https://doi.org/10.1016/J.COMPSTRUCT.2022.115838. Sep.
[70] Kuhn P, Catalanotti G, Xavier J, Ploeckl M, Koerber H. Determination of the crack resistance curve for intralaminar fiber tensile failure mode in polymer composites under high rate loading. Compos Struct 2018;204:276–87. https://doi.org/10.1016/J.COMPSTRUCT.2018.07.039. Nov.

[71] Yu B, et al. Characterizing and predicting the relationship between translaminar fracture toughness and pull-out length distributions under distinct temperatures. Philos Trans R Soc A 2023;381(2240). https://doi.org/10.1098/RSTA.2021.0220. Jan.

[72] L. Marín, E.V. Gonz Alez, P. Maimí, D. Trias, and P.P. Camanho B A Amade, "Hygrothermal effects on the translaminar fracture toughness of cross-ply carbon/epoxy laminates: failure mechanisms," 2015, doi:10.1016/j.compscitech.2015.10.020.

[73] Teixeira RF, Pinho ST, Robinson P. Thickness-dependence of the translaminar fracture toughness: experimental study using thin-ply composites. Compos Appl Sci Manuf 2016;90:33–44. https://doi.org/10.1016/j.compositesa.2016.05.031. Nov.